COMPARISON OF UAV IMAGERY-DERIVED POINT CLOUD TO TERRESTRIAL LASER SCANNER POINT CLOUD

S. Peterson [1], J. Lopez[1], R. Munjy[1]

[1] Department of Civil and Geomatics Engineering, Lyles College of Engineering, California State University, Fresno, 2320 E San Ramon Ave., Fresno, CA 93740, USA – (scpeterson@csufresno.edu, jakelopez1@mail.fresnostate.edu, riadhm@csufresno.edu)

KEY WORDS: Point Cloud, Terrestrial Laser Scanner, Unmanned Aerial Vehicle, DSM, Photogrammetry, GNSS, Leveling

ABSTRACT:

A small unmanned aerial vehicle (UAV) with survey-grade GNSS positioning is used to produce a point cloud for topographic mapping and 3D reconstruction. The objective of this study is to assess the accuracy of a UAV imagery-derived point cloud by comparing a point cloud generated by terrestrial laser scanning (TLS). Imagery was collected over a 320m by 320m area with undulating terrain, containing 80 ground control points. A SenseFly eBee Plus fixed-wing platform with PPK positioning with a 10.6mm focal length and a 20MP digital camera was used to fly the area. Pix4Dmapper, a computer vision based commercial software, was used to process a photogrammetric block, constrained by 5 GCPs while obtaining cm-level RMSE based on the remaining 75 checkpoints. Based on results of automatic aerial triangulation, a point cloud and digital surface model (DSM) (2.5 cm/pixel) are generated and their accuracy assessed. A bias less than 1 pixel was observed in elevations from the UAV DSM at the checkpoints. 31 registered TLS scans made up a point cloud of the same area with an observed horizontal root mean square error (RMSE) of 0.006m, and negligible vertical RMSE. Comparisons were made between fitted planes of extracted roof features of 2 buildings and centreline profile comparison of a road in both UAV and TLS point clouds. Comparisons showed an average +8-cm bias with UAV point cloud computing too high in two features. No bias was observed in the roof features of the southernmost building.

1. INTRODUCTION

Generating dense point clouds from photography from small unmanned aerial vehicles (UAV) has been an attractive method for mapping and 3D reconstruction due to its efficiency and largely automated workflow. UAV imagery-derived point clouds over large areas would be preferred over point clouds generated by terrestrial laser scanning (TLS) given comparable results for economic and efficiency considerations. Past studies on the topic of UAV imagery-derived point cloud accuracy assessment using TLS point clouds for comparison have presented varying results. Applications requiring higher accuracy and precision for mapping and 3D reconstruction of built and hardscaped features require a precise point cloud comparison analysis.

There is gap in the literature regarding the use of UAV imagery combined with survey-grade global navigation satellite system (GNSS) positioning combined with a highly accurate dense control network for deriving high accuracy imagery-derived point clouds for mapping hardscaped features. The work of Ostrowski and colleagues (Ostrowski et al., 2014) compared rotorcraft UAV imagery-derived point clouds generated by different software packages. The site limited ground control distribution geometry and quantity, which limited checkpoint validation to few points and did not employ TLS for comparisons. A study mapping a hardscaped dike found TLS and UAV-derived point clouds to be comparable, however the UAV did not have on-board, dual-frequency GNSS positioning to precisely record exposure stations for adjustment (Naumann et al., 2013). Ouedraogo and colleagues compared data collected over an agricultural watershed area, a site that lacked built features (Ouédraogo et al., 2014). Reshetyuk and Mårtensson performed a study showing that a computer vision-based software resolved UAV imagery-derived elevations with higher certainty in flat terrain portions of a quarry site than a non-computer vision-based software. They also showed that the opposite was the case over undulating terrain (Reshetyuk and Mårtensson, 2016). A comparison was performed by a point-to-point difference analysis between clouds (Eling et al., 2016). Another comparison was made between DSM surfaces generated by data collected in sub-optimal positioning conditions where high-elevation terrain obstructions affected the establishment of ground control quality (Jaud et al., 2016). Gruszczyński and colleagues compared UAV and TLS point clouds over grass-vegetated terrain with efforts to minimize the impact of the vegetation on elevation extraction (Gruszczyński et al., 2017). The study focused on interpolation and point filtration methods finding the UAV imagery-derived point cloud to be more accurate in all cases noting the more consistent point density over TLS method.

Various factors and parameters affect the photogrammetric model required for dense point cloud generation. Bundle block adjustments of UAV imagery have been thoroughly studied throughout the literature. These factors were considered in flight planning for this study including ground control accuracy and distribution (Agüera-Vega et al., 2016, James et. al., 2016), influence of on-board UAV dual-frequency GNSS positioning capabilities and flight planning (Gerke and Przybilla, 2016). On-board, dual-frequency GNSS with accuracy ranging from 2 to 3cm reduces the amount of ground control required for precise mapping (Agüera-Vega et al., 2016, Benassi et al., 2017) when applied as constraints in the adjustment. It has been shown that although on-board GNSS receiving of a UAV contributes to the overall accuracy of the image block, high-accuracy ground control surveyed by total station or dual-frequency static or kinematic GNSS is required for absolute orientation of the block to optimize network accuracy and mitigate block deformation (Gerke and Przybilla, 2016). Gerke and Przybilla looked at ground control distribution and cross-flights using a similarly capable UAV platform to this study. Ground control for this study were surveyed with high accuracy, and stabilization was observed in the adjustment results using a minimum five control point-distribution. Additionally, the effect of cross-flights on the adjustment were found negligible.

This contribution has been peer-reviewed. The double-blind peer-review was conducted on the basis of the full paper.
https://doi.org/10.5194/isprs-annals-IV-2-W5-149-2019 | © Authors 2019. CC BY 4.0 License.

This study focuses on the analysis of a dense point cloud derived from UAV imagery based on bundle block adjustment (BBA) results using five ground control points by comparison with a point cloud generated from TLS. Aerial triangulation (AT) accuracy assessment was determined horizontally by the orthomosaic and vertically by the digital surface model (DSM). AT results statistics were based on a large sample of highly accurate ground control that were omitted from the adjustment and designated as checkpoints. This study also inherently tests the integrity of the employed commercial UAV photogrammetry software in the omission of checkpoints from the project completely. This procedural decision was made due to proprietary processing methods of commercial computer-vision-based software. The aim of this study is to determine the ability of a small UAV with survey-grade GNSS positioning and 20MP digital camera to generate a 3D point cloud sufficiently accurate to model hardscaped and build features within a precise control network. To assess the accuracy of the imagery-derived point cloud a TLS point cloud is used as ground truth and hardscaped and built features are extracted and compared.

1.1 Control

To assess the quality of the UAV block using Pix4Dmapper from an east-west oriented flight of an eBee UAV system, a 320m x 320m control field was established in the San Joaquin Experimental Range (SJER), which is located approximately 32 km north of the California State University, Fresno campus. The terrain features varying topography with sparse vegetation, structures, and paved and unpaved roads. A total of 81 ground control point locations were designed in an approximate 40-m grid pattern (Figure 1). The horizontal positioning was established using static GNSS method (base station shown in Figure 1) at two different collection times. Differential levelling was performed with a digital level to establish the control vertical positions. The points were placed and surveyed with 0.010 m horizontal and 0.003 m vertical accuracy. Flight targets (80, circular, black and white, diameter = 46 cm) were placed atop the surveyed control points and measured in the imagery.

UAV imagery bundle block adjustments (BBA) for control distributions of 0 (i.e. only aircraft RTK positions), 5, 7, and 9 control points in a symmetrical pattern such as illustrated in figure 1. Results for these distributions showed a stabilization of results at 5 control points.

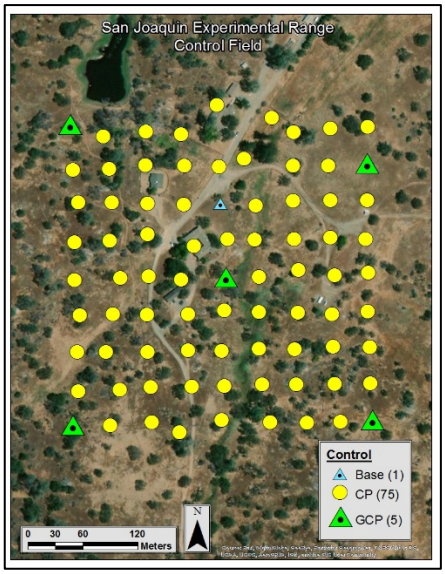

Figure 1: Site and ground control ponit and ground control point checkpoint layout

1.2 TLS System

The Leica P20 ScanStation and the Lecia C10 ScanStation were the 2 TLS systems used to create the ground truth point cloud for the selected site. The Leica P20 ScanStation has a range of 120m, a 3D positional accuracy of 0.3cm at 50m distant and 0.006m at 100m distant, and a ±0. 2cm standard deviation up to 50m for target acquisition (Leica, 2013). The Leica C10 ScanStation has a range of 300m, a 3D positional accuracy of 0.6cm, and a ±0.2cm standard deviation for target acquisition (Leica, 2011). 31 setups were completed by resection using HDS (high definition scanning) targets to create a complete model of the selected site. The overall mean absolute error of the complete point cloud registration was 0.6cm, with an average vertical error of 0.0cm and a vertical standard deviation (STD) of ±0.2cm. Average point spacing is 1.1cm and 8214 m^{-2} point density. The ScanStations were set to an average of 6mm spacing at 10m at while performing full 360° horizontal by 270° vertical scans.

1.3 UAV System

The senseFly eBee Plus UAS is a hand-launched, fixed-wing, survey-grade, complete photogrammetric system with a built-in RTK/PPK functionality that is activated on-demand. The system has dual GPS frequency (L1 and L2) and integrated IMU. The imaging system consists of 20 MB (5472 x 3648) RGB CMOS sensor with global mechanical shutter. It has a 2.4 micrometer pixel size and 10.6 mm focal length (senseFly, 2016).

1.4 UAV Flights

The UAV flight was flown in an east-west oriented direction with design 70% forward lap and 80% side lap. The average ground sampling distance (GSD) was 2.45 cm with an average flying height 114m above ground level (AGL). Table 1 provides a summary of the flight parameters and conditions.

Date	Flying Height (m AGL)	GSD (cm)	Orientation	Photographs	Temp (C)	Wind (km/h)	Wind Dir (deg)
6/25/2018	114	2.45	E-W	293	38	15	1.1

Table 1. Flight parameters

2. DATA PROCESSING

2.1 UAV Imagery Processing and Adjustment

The imagery was processed in Pix4Dmapper software. The total number of photographs processed was 293. A priori standard deviations for initial exterior orientation positions were set to 2.3cm and 2.5cm in the horizontal and vertical respectively. Five ground control points (GCP in Figure 1) were included in the Pix4D BBA while the remaining 75 points were designated as checkpoints (CP). The CP's were omitted from the project altogether and measured outside of the software in the orthomosaic and DSM for validation of the BBA results (Table 2). Omission of CP's from the Pix4D project was performed in this way because it was discovered that checkpoint errors reported by the Pix4D were not consistent between being included or excluded from the project. Therefore, the BBA results unveiled by the CP's may not be influenced by unknown software processes. A priori GCP horizontal and vertical accuracy was set at 1.0 cm and 1.0 cm respectively. The control points were then located and measured in the imagery. The GCP's were seen by a range of 6 to 10 images. Keypoint candidates for automatic tie points were extracted at full image scale (i.e. original image size). Camera self-calibration was performed to estimate principal distance, principal point offset, three parameters, R1, R2, R3 of symmetrical radial distortion, and two parameters T1, T2 of tangential distortion. A dense point cloud was generated at full image scale (Figure 2).

Figure 2: UAV-derived dense point cloud (full image scale sampling)

An orthomosaic was then created with pixel resolution set to 2.5 cm. Finally, a digital surface model was generated with 2.5 cm resolution using inverse distance weighting interpolation.

Flight targets in the orthomosaic were located and measured in the projected coordinates to extract the horizontal position in ArcMap software. The horizontal position obtained from the orthomosaic was used to extract an elevation value from the DSM. Table 2 presents a CP position error summary of the orthomosaic and DSM based on the 75 points.

		RMSE (cm)				Average Error (cm)				Error Range (cm)			
GCP	CP	x	y	z	xy	x	y	z	xy	x	y	z	xy
5	75	1.27	1.13	2.17	1.70	-0.10	-0.50	-1.62	1.50	6.12	5.25	7.63	3.51

Table 2. UAV Orthomosaic and DSM accuracy statistics based on 75 checkpoints.

The vertical error shows a bias of -1.62 cm. Figure 3 shows a contour map displaying the elevation errors observed in the DSM. The point showing a large positive elevation difference was likely caused by interpolation limitations at the target taking nearby lower elevations into account. The target was elevated about 4 cm above ground due to the hard bedrock preventing the target to be flush with the ground.

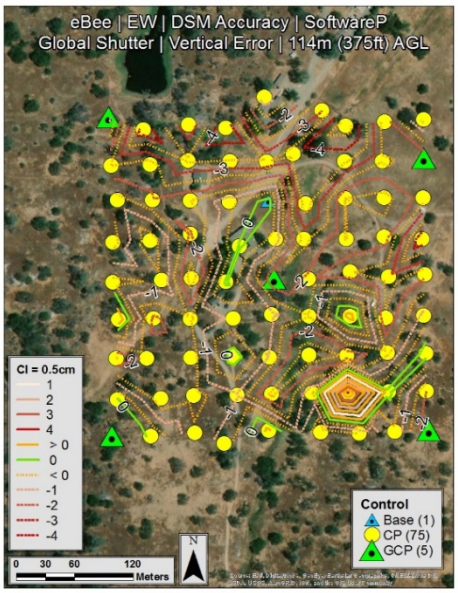

Figure 3. UAV-derived DSM (2.5 cm/pix) vertical error contour map using Pix4D with 5 GCP

2.2 TLS Point Cloud Processing

Leica Cyclone was used to register each of 31 individual scans to the control field (Figure 1). There were 31 setups and established by resection using high definition scanning (HDS) targets to create a model of the selected site (Figure 2). Each scan setup used a minimum of 3 control points to solve for the position of the scanner. Resection was applied to the TLS setup to resolve the 3D position of the scan sensor station. Orientation was derived by the relative position of the scanner coordinates with respect to the control points with the vertical component established as being parallel to the gravity vector (perpendicular to the horizontal plane). The TLS point cloud was used as the ground truth upon which the comparison with the UAV imagery-derived point cloud was made (Figure 3).

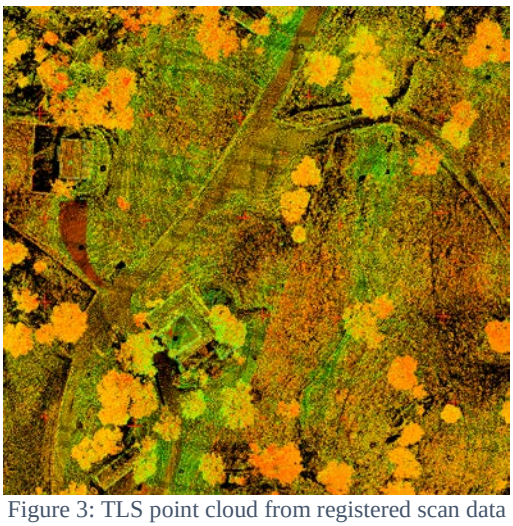

Figure 3: TLS point cloud from registered scan data

The overall mean absolute error of the complete point cloud registration was 0.006m horizontally and negligible vertical error ±0.002m. The ScanStations were set to an average of 6mm spacing at 10m while performing full 360° horizontal by 270° vertical scans.

Given the results from the UAV's and TLS's transformation to the control field, no translations nor shifts were necessary to superimpose the UAV's and TLS's point clouds. The remaining comparisons were made in the vertical plane.

3. RESULTS

3.1 Point Cloud Comparison by Plane Fitting

There were temporal differences with regards to the terrain between scanning collections. Field grasses and trees were all at different growing phases during each set of data collection. Due to these differences, hardscape features were necessary to make accurate point cloud comparisons. Two buildings within the control site in both UAV and TLS point clouds were features extracted for comparison. A total of 8 planes were fit to building roof features extracted from each point cloud (Figure 4) using Leica Cyclone software. The topography provided the scanner station with elevated vantage point to capture the roof with useable angle-of-incidence and sufficient point density for comparison against the UAV point cloud.

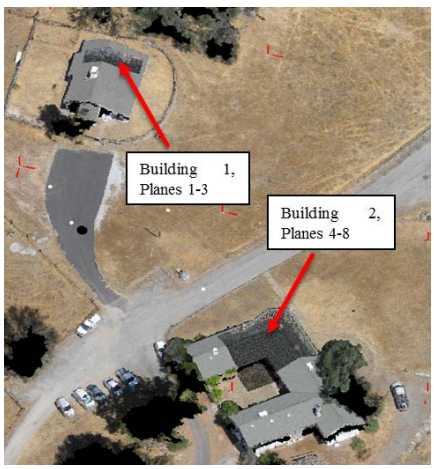

Figure 4: UAV point cloud perspective view.

The roof faces of building 1 (planes 1-3) were oriented E-W. The statistics of the plane-fitting for the roof faces of building 1 are presented in Table 3.

Terrestrial Laser Scanning Point Cloud Data

Plane	Fitted Percentage of Points Used	Plane Fit Quality (cm) Error Mean	Error Std Deviation	Absolute Error Mean	Maximum Absolute Error	Elevation Angle (West to East)
#1	99.97%	0.0	0.3	0.2	1.1	20°29'44"
#2	99.35%	0.0	0.3	0.3	1.2	20°42'26"
#3	58.47%	-0.1	0.5	0.4	1.2	13°01'04"

UAV Photogrammetric Derived Point Cloud Data

Plane	Fitted Percentage of Points Used	Plane Fit Quality (cm) Error Mean	Error Std Deviation	Absolute Error Mean	Maximum Absolute Error	Elevation Angle (West to East)
#1	48.65%	0.1	0.7	0.6	1.2	20°54'02"
#2	53.62%	0.1	0.7	0.6	1.2	20°41'27"
#3	61.12%	0.1	0.7	0.6	1.2	13°11'41"

Table 3. Plane-fitting results for TLS and UAV for building 1.

The UAV point cloud exhibited noise with range of about 15cm. Also, there was a vertical bias of approximately 8cm between points on the roof of building 1 (Figure 5).

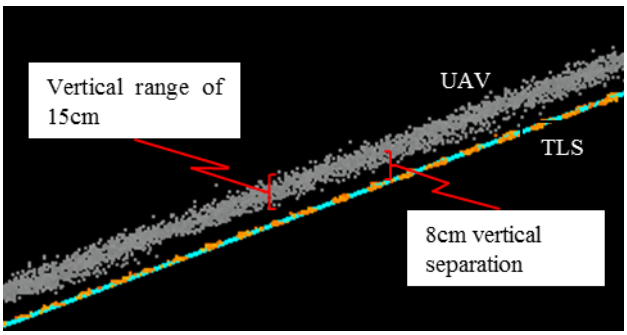

Figure 5. Building 1. UAV point cloud noise and vertical bias compared to TLS.

The roof faces of building 2 (planes 4-8) were oriented NW-SE and NE-SW (Figure 6).

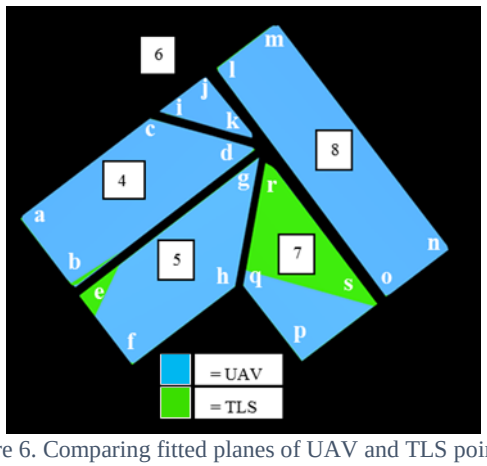

Figure 6. Comparing fitted planes of UAV and TLS points to roof faces of building 2.

The interface between color change represents intersection of fitted planes. The statistical summary of the plane-fitting for roof faces of building 2 is given in Table 4.

Terrestrial Laser Scanning Point Cloud Data

Plane	Fitted Percentage of Points Used	Plane Fit Quality (cm) Error Mean	Error Std Deviation	Absolute Error Mean	Maximum Absolute Error	Elevation Angle (West to East)
#4	89.96%	0.0	0.5	0.4	1.2	20°17'53"
#5	98.41%	0.0	0.4	0.3	1.2	20°25'48"
#6	92.75%	0.0	0.4	0.3	1.2	26°09'20"
#7	99.15%	-0.1	0.4	0.4	1.2	18°24'50"
#8	87.26%	0.0	0.5	0.4	1.2	22°26'13"

UAV Photogrammetric Derived Point Cloud Data

Plane	Fitted Percentage of Points Used	Plane Fit Quality (cm) Error Mean	Error Std Deviation	Absolute Error Mean	Maximum Absolute Error	Elevation Angle (West to East)
#4	34.13%	0.0	0.7	0.6	1.2	19°19'03"
#5	40.95%	0.1	0.7	0.6	1.2	20°18'53"
#6	65.29%	0.1	0.6	0.5	1.2	26°27'11"
#7	50.51%	-0.2	0.6	0.6	1.2	18°13'54"
#8	45.41%	-0.2	0.6	0.6	1.2	22°15'22"

Table 4. Plane fitting results for UAV and TLS for building 2 of Figure 6.

Each fitted plane produced results in fit quality as well as a normal vector to that plane. The slope of each roof top was derived from the calculated normal vector of each plane. The slopes computed for each point cloud were compared.

The UAV point cloud data were noisy with a range of 15cm on planar surfaces. The noise was observed as Cyclone used an average of half of the measured data to fit planes to the roofs. Regardless of the rejected points used to compute the planes, the fitted planes reached a maximum absolute error of no more than 1.2cm. The computed elevation angles by UAV were comparable to the TLS data.

The UAV planes were higher on most of the compared faces of roofs of building 2. However, there was not a consistent bias as detected in building 1. Also, as shown in Table 4, Plane #4 did not have matching elevation angles, resulting in different separation distances of the planes. All corners of planes #5 and #7 match one another vertically within 2.2cm on all corners (Table 5), confirming the DSM accuracy based on the checkpoints noting a vertical accuracy of 2.5cm (Table 2). Inconsistent separations ranged from 2.0m to 8.0cm on all other planes on building 2, showing an inconsistent relationship with the TLS data.

Difference in Elevation (cm)

Plane #4	Plane #5	Plane #6	Plane #7	Plane #8
a - 7.0	e - 0.2	i - 4.6	l - 2.3	p - 1.4
b - 0.0	f - 0.7	j - 6.0	m - 3.4	q - 0.3
c - 8.2	g - 1.0	k - 5.5	n - 6.7	r - 2.2
d - 1.4	h - 1.4		o - 5.6	s - 0.1

Table 5. Plane fitting differences at corners a-s of building 2 of Figure 6.

3.2 Point Cloud Comparison by Centerline Profile of Road

A second method of point cloud comparison involved extracting a centerline profile along a non-uniform surface. Figure 7 shows the alignment of the road with stations at which elevation comparisons were made.

Figure 7. Road centerline and stations extracted from both point clouds for comparison.

The road (asphalt) was extracted from the point clouds with an average width of 3m. The elevation range of the road was 2.5m. In all measurements of the road, the UAV data was above the TLS data - a bias of an average of +8.0cm – the same bias found in the analysis of building 1 by plane comparison (Figure 8). However, the vertical geometry of the UAV data matched the vertical geometry of the TLS data.

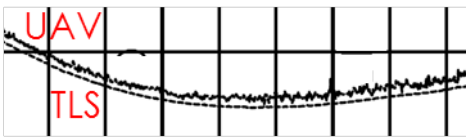

Figure 8. Sample of UAV point cloud noise and vertical separation from TLS.

Difference values computed at the stations are shown in the profile graph of Figure 9.

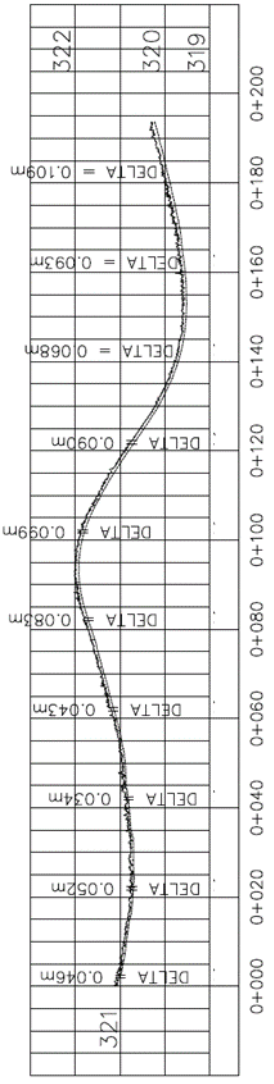

Figure 9. Elevation differences computed at stations along the road centreline (all values in meters).

4. CONCLUSIONS

The UAV flight mission was oriented east-west. UAV imagery processed at full image scale and adjusted in Pix4Dmapper using 5 GCP produced a root mean square error (RMSE) value of 1.70 cm horizontally based on 75 checkpoints. The vertical accuracy of the model based on elevations extracted from the DSM produced an RMSE of 2.17 cm. The dense point cloud generated based on these automatic aerial triangulation results was compared to a point cloud generated by TLS. The TLS data registered to each control point at an RMSE of 0.4 cm and 0.2 cm horizontally and vertically respectively. Both UAV and TLS produce accurate models based on their respective error summaries.

However, a substantial bias of 8cm was observed between UAV and TLS point clouds when comparing fitted planes to the roof faces of building 1. A bias of roughly similar magnitude was also observed along more than 200m of road. In contrast, substantially lesser differences in elevations were observed when comparing planes fitted to the roof faces of building 2; and, in a couple locations the elevation difference converged. This observation suggests a possible correlation between UAV flight trajectory orientation and feature orientation and/or slope, but further research is required to explain this.

The ability of the UAV imagery to compute slopes of planes and estimate vertical geometry of non-uniform surfaces is confirmed in this study.

ACKNOWLEDGEMENTS

This research is sponsored by the California Department of Transportation (Caltrans) and California State University, Fresno.

REFERENCES

Agüera-Vega, F., Carvajal-Ramírez, F., Martínez-Carricondo, P., 2017. Assessment of photogrammetric mapping accuracy based on variation ground control points number using unmanned aerial vehicle. *Measurement*, 98, 221-227.

Benassi, F., Dall'Asta, E., Diotri, F., Forlani, G., Morra di Cella, U., Roncella, R., Santise, M., 2017. Testing accuracy and repeatability of UAV blocks oriented with GNSS-supported aerial triangulation. *Remote Sensing*, 9(2), 172.

Eling, C., Klingbeil, L., Wieland, M., Kuhlmann, H., 2016. Towards deformation monitoring with uav-based mobile mapping systems. *Proc., 3rd Joint Int. Symp. on Deformation Monitoring (JISDM)*, TU Wien, Vienna.

Gerke, M., Przybilla, H.-J., 2016. Accuracy Analysis of Photogrammetric UAV Image Blocks: Influence of Onboard RTKGNSS and Cross Flight Patterns. *Photogrammetrie – Fernerkundung – Geoinformation* (PFG), 2016 (1), 17-30. doi.org/10.1127/pfg/2016/0284.

Gruszczyński, W., Matwij, W., Ćwiąkała, P. J. I. J. o. P., Sensing, R., 2017. Comparison of low-altitude UAV photogrammetry with terrestrial laser scanning as data-source methods for terrain covered in low vegetation. *ISPRS Journal of Photogrammetry and Remote Sensing*. 126, 168-179. doi.org/10.1016/j.isprsjprs.2017.02.015.

James, M. R., Robson, S., d'Oleire-Oltmanns, S., Niethammer, U., 2017. Optimising UAV topographic surveys processed with structure-from-motion: Ground control quality, quantity and bundle adjustment. *Geomorphology*, 280, 51-66.

Jaud, M., Passot, S., Le Bivic, R., Delacourt, C., Grandjean, P., Le Dantec, N., 2016. Assessing the accuracy of high resolution digital surface models computed by PhotoScan® and MicMac® in sub-optimal survey conditions. *Remote Sensing*, 8(6), 465.

Leica, 2011. Leica ScanStation C10: The All-in-One Laser Scanner for Any Application. Leica Geosystems AG, Heerbrugg Switzerland.

Leica, 2013. Leica ScanStation P20: Industry's Best Performing Ultra-High Speed Scanner. Leica Geosystems AG, Heerbrugg Switzerland.

Naumann, M., Geist, M., Bill, R., Niemeyer, F., Grenzdörffer, G., 2013. Accuracy comparison of digital surface models created by unmanned aerial systems imagery and terrestrial laser scanner.

International Archives of the Photogrammetry, Remote Sensing and Spatial Information Sciences, 40(5 W2).

Ostrowski, S., Jóźków, G., Toth, C., Vander Jagt, B., 2014. Analysis of Point Cloud Generation from UAS Images. *ISPRS Annals of Photogrammetry, Remote Sensing & Spatial Information Sciences* II-1, 45-51. doi.org/10.5194/isprsannals-II-1-45-2014, 2014.

Ouédraogo, M. M., Degré, A., Debouche, C., Lisein, J., 2014. The evaluation of unmanned aerial system-based photogrammetry and terrestrial laser scanning to generate DEMs of agricultural watersheds. *Geomorphology*, 214, 339-355.

Reshetyuk, Y., Mårtensson, S. G., 2016. Generation of highly accurate digital elevation models with unmanned aerial vehicles. *The Photogrammetric Record*, 31(154), 143-165.

senseFly, 2016. eBee Plus: Aerial Efficiency, Photogrammetric Accuracy. <https://optron.com/sensefly/products/ebee-plus/#related-media>. (01/16/2019).